Inorg. Chem. **2004**, *43*, 144–154

Structure and Magnetism of the Tetra-Copper(II)-Substituted Heteropolyanion $[Cu_4K_2(H_2O)_8(\alpha\text{-}AsW_9O_{33})_2]^{8-}$†

Ulrich Kortz,*,‡ Saritha Nellutla,§ Ashley C. Stowe,§ Naresh S. Dalal,*,§ Johan van Tol,§,|| and Bassem S. Bassil‡

School of Engineering and Science, International University Bremen, P.O. Box 750 561, 28725 Bremen, Germany, Department of Chemistry and Biochemistry, Florida State University, and National High Magnetic Field Laboratory, Center for Interdisciplinary Magnetic Resonance, Tallahassee, Florida 32306-4390

Received June 18, 2003

The novel heteropolyanion $[Cu_4K_2(H_2O)_8(\alpha\text{-}AsW_9O_{33})_2]^{8-}$ (**1**) has been synthesized and characterized by IR spectroscopy, elemental analysis, and magnetic studies. Single-crystal X-ray analysis was carried out on $\{K_7Na\text{-}[Cu_4K_2(H_2O)_6(\alpha\text{-}AsW_9O_{33})_2]\cdot 5.5H_2O\}_n$ (**K_7Na-1**), which crystallizes in the tetragonal system, space group $P\bar{4}2_1m$, with $a = 16.705(4)$ Å, $b = 16.705(4)$ Å, $c = 13.956(5)$ Å, and $Z = 2$. Interaction of the lacunary $[\alpha\text{-}AsW_9O_{33}]^{9-}$ with Cu^{2+} ions in neutral, aqueous medium leads to the formation of the dimeric polyoxoanion **1** in high yield. Polyanion **1** consists of two $\alpha\text{-}AsW_9O_{33}$ units joined by a cyclic arrangement of four Cu^{2+} and two K^+ ions, resulting in a structure with C_{2v} symmetry. All copper ions have one terminal water molecule, resulting in square-pyramidal coordination geometry. Three of the copper ions are adjacent to each other and connected via two μ_3-oxo bridges. EPR studies on **K_7Na-1** and also on $Na_9[Cu_3Na_3(H_2O)_9(\alpha\text{-}AsW_9O_{33})_2]\cdot 26H_2O$ (**Na_9-2**) over 2–300 K yielded *g* values that are consistent with a square-pyramidal coordination around the copper(II) ions in **1** and **2**. No hyperfine structure was observed due to the presence of strong spin exchange, but fine structure was observed for the excited ($S^T = 3/2$) state of **Na_9-2** and the ground state ($S^T = 1$) of **K_7Na-1**. The zero-field (*D*) parameters have also been determined for these states, constituting a rare case wherein one observes EPR from both the ground and the excited states. Magnetic susceptibility data show that **Na_9-2** has antiferromagnetically coupled Cu^{2+} ions, with $J = -1.36 \pm 0.01$ cm^{-1}, while **K_7Na-1** has both ferromagnetically and antiferromagnetically coupled Cu^{2+} ions ($J_1 = 2.78 \pm 0.13$ cm^{-1}, $J_2 = -1.35 \pm 0.02$ cm^{-1}, and $J_3 = -2.24 \pm 0.06$ cm^{-1}), and the ground-state total spins are $S^T = 1/2$ in **Na_9-2** and $S^T = 1$ in **K_7Na-1**.

Introduction

The existence of polyoxometalates has been known for almost 200 years, but the first structural details were only revealed in the last century.[1,2] Meanwhile it has been widely recognized that this class of metal−oxygen cluster species exhibits a unique variety of structures and properties that make them useful in catalysis, materials science, and medicine.[3−8]

Polyoxoanions are formed by the early transition metals of groups V and VI in their highest oxidation states (e.g., V^{5+}, W^{6+}) by condensation reactions in aqueous, acidic medium. The mechanism of formation of polyoxometalates

* Authors to whom correspondence should be addressed. E-mail: u.kortz@iu-bremen.de (U.K.); dalal@chemmail.chem.fsu.edu (N.S.D.). Fax: +49-421-200 3229 (U.K.); (850) 644-3398 (N.S.D.).

† Dedicated to Prof. B. Krebs on the occasion of his 65th birthday.

‡ International University Bremen.

§ Florida State University.

|| Center for Interdisciplinary Magnetic Resonance.

(1) Berzelius, J. *Poggendorff's Ann. Phys.* **1826**, *6*, 369.

(2) (a) Keggin, J. F. *Nature* **1933**, *131*, 908. (b) Keggin, J. F. *Proc. R. Soc. London, A* **1934**, *144*, 75.

(3) Pope, M. T. *Heteropoly and Isopoly Oxometalates*; Springer-Verlag: Berlin, 1983.

(4) Pope, M. T.; Müller, A. *Angew. Chem., Int. Ed. Engl.* **1991**, *30*, 34.

(5) *Polyoxometalates: From Platonic Solids to Anti-Retroviral Activity*; Pope, M. T., Müller, A., Eds.; Kluwer: Dordrecht, The Netherlands, 1994.

(6) *Polyoxometalates*; Hill, C., Ed. *Chem. Rev.* **1998**, *98*.

(7) *Polyoxometalate Chemistry: From Topology via Self-Assembly to Applications*; Pope, M. T., Müller, A., Eds.; Kluwer: Dordrecht, The Netherlands, 2001.

(8) *Polyoxometalate Chemistry for Nano-Composite Design*; Yamase, T., Pope, M. T., Eds.; Kluwer: Dordrecht, The Netherlands, 2002.

10.1021/ic034697b CCC: $27.50
Published on Web 12/09/2003

is difficult to understand, because even very large and complex structures (e.g., $[As_{12}Ce_{16}(H_2O)_{36}W_{148}O_{524}]^{76-}$)[9] can be synthesized in one-pot reactions by interaction of the composing elements without the need for any polyoxoanion precursor species. Therefore, the discovery of novel polyoxoanions with completely unexpected structures and properties is not uncommon. In polyoxoanion chemistry it is usually not possible to design a multistep synthetic sequence with its associated conditions, unlike in organic chemistry. As a result the rational synthesis and derivatization of polyoxometalates remains a challenge.

The class of As(III)-containing polyoxotungstates has been known for a long time.[10] The presence of a lone pair of electrons on the heteroatom does not allow the closed Keggin unit to form, and therefore, many structures could not be easily predicted. However, by using single-crystal X-ray diffraction the geometries of some tungstoarsenate(III) species have been revealed. It is useful to distinguish nonsubstituted from transition-metal-substituted and rare-earth-metal-substituted (lanthanides and uranium) tungstoarsenates(III). The first subclass is represented by $[H_2AsW_{18}O_{60}]^{7-}$, $[As_2W_{21}O_{69}(H_2O)]^{6-}$, $[AsW_8O_{30}AsOH]^{7-}$, $[As_4W_{20}O_{72}(H_2O)_2]^{12-}$, $[As_2W_{19}O_{67}(H_2O)]^{14-}$, and $[As_6W_{65}O_{217}(H_2O)_7]^{26-}$.[11] The second subclass is represented by $[NH_4As_4W_{40}O_{140}Co_2(H_2O)_2]^{23-}$, $[As_2W_{18}Cu_3O_{66}(H_2O)_2]^{12-}$, $[As_2CoW_{20}O_{68}(OH_2)_2]^{8-}$, $[(Hg_2)_2WO(H_2O)(AsW_9O_{33})_2]^{10-}$, $[\{(C_6H_5Sn)_2O\}_2H(AsW_9O_{33})_2]^{9-}$, $[M_3(H_2O)_3(\alpha\text{-}AsW_9O_{33})_2]^{12-}$ (M = Cu^{2+}, Zn^{2+}), $[WO(H_2O)M_2(H_2O)_2(\alpha\text{-}AsW_9O_{33})_2]^{10-}$ (M = Zn^{2+}, Mn^{2+}, Co^{2+}), $[M_3(H_2O)_3(\alpha\text{-}AsW_9O_{33})_2]^{12-}$ (M = Mn^{2+}, Co^{2+}), $[(VO)_3(\alpha\text{-}AsW_9O_{33})_2]^{11-}$, and $[As_2W_{19}(H_2O)\{Ni(H_2O)\}_2O_{67}]$.[10-12] The third subclass is represented by $As_{12}Ln_{16}(H_2O)_{36}W_{148}O_{524}]^{76-}$ (Ln = La, Ce), $[As_2Ln_2(H_2O)W_{29}O_{103}]^{17-}$ (Ln = La, Ce), $[Ce_4(H_2O)_{4-4x}(AsW_9O_{33})_4As(WO_3)_{2+x}(WO_5)]^{25-}$ ($x < 0.5$), $[(H_2O)_{11}Ln^{III}(Ln^{III}{}_2OH)(AsW_9O_{33})_4(WO_2)_4]^{20-}$ (Ln = Ce, Nd, Sm, Gd), $[M^m(H_2O)_{10}(Ln^{III}{}_2OH)_2(AsW_9O_{33})_4(WO_2)_4]^{(18-m)-}$ (Ln = La, Ce, Gd and M = Ba, K, none), $[(UO_2)_3(H_2O)_5As_3W_{29}O_{104}]^{19-}$, $[(UO_2)_3(H_2O)_6As_3W_{30}O_{105}]^{15-}$, $[(UO_2)_3(H_2O)_4As_3W_{26}O_{94}]^{17-}$, $[Na(UO_2)_3(OH)(H_2O)_6As_4W_{40}O_{140}(WO)]^{18-}$, $[K\subset\{Eu(H_2O)_2(\alpha\text{-}AsW_9O_{33})\}_6]^{35-}$, $[Cs\subset\{Eu(H_2O)_2(\alpha\text{-}AsW_9O_{33})\}_4]^{23-}$, and $[YbAs_2W_{20}O_{68}(H_2O)_3]^{7-}$.[9,13]

It can be noticed that almost all transition-metal-substituted tungstoarsenates(III) are dimeric and of the sandwich type. The first copper-containing derivative of this type was structurally characterized in 1982 by Hervé and coworkers.[12b] Single-crystal X-ray analysis of the potassium salt of $[Cu_3(H_2O)_2(\alpha\text{-}AsW_9O_{33})_2]^{12-}$ revealed a sandwich-type structure with three Cu^{2+} ions linking two $[\alpha\text{-}AsW_9O_{33}]^{9-}$ units. Surprisingly, the three copper ions were not equivalent, because of a difference in their coordination geometry. The authors identified a glide of one AsW_9 subunit with respect to the other which they explained to be a result of lone-pair/lone-pair repulsion of the two As(III) atoms.

Recently, Kortz et al. determined the structure of the sodium salt of the copper-containing tungstoarsenate(III), $Na_{12}[Cu_3(H_2O)_2(\alpha\text{-}AsW_9O_{33})_2]\cdot 32H_2O$, and did not observe the above distortion.[12f] The polyanion $[Cu_3(H_2O)_3(\alpha\text{-}AsW_9O_{33})_2]^{12-}$ exhibited D_{3h} symmetry, indicating that all three copper centers were equivalent.

Some time ago, Siedle et al. reported the powder EPR properties of the sodium salt $Na_{12}[Cu_3(H_2O)_3(\alpha\text{-}AsW_9O_{33})_2]$ and the mixed sodium/potassium salt $Na_{3.2}K_{8.8}[Cu_3(H_2O)_3(\alpha\text{-}AsW_9O_{33})_2]$.[14] However, these authors based the data interpretation on the polyoxoanion structure of the potassium salt of Hervé et al., not being aware of the significant structural differences of the Na and K salts described above. More recently, Cho and So reported that the powder EPR properties of the "Hervé structure" were identical to those reported by Siedle et al.[15] This would mean that the structural differences of the polyoxoanions in the K and Na salts ($[Cu_3(H_2O)_2(\alpha\text{-}AsW_9O_{33})_2]^{12-}$ vs $[Cu_3(H_2O)_3(\alpha\text{-}AsW_9O_{33})_2]^{12-}$) have no effect on their EPR properties, which would normally be unexpected.

We thus decided (a) to reinvestigate the magnetic properties of the potassium salt of the tri-copper-substituted tungstoarsenate(III) in detail and (b) to incorporate more than three copper ions in this polyanion structure.

Experimental Section

Synthesis. The precursor polyanion $[\alpha\text{-}AsW_9O_{33}]^{9-}$ was synthesized according to the published procedure, and the potassium salt was isolated by addition of solid KCl.[10a,16] The identity of the polyanion in the product was confirmed by infrared spectroscopy. The crystalline $Na_9[Cu_3Na_3(H_2O)_9(\alpha\text{-}AsW_9O_{33})_2]\cdot 26H_2O$ (**Na_9-2**) was synthesized according to the published procedure and then used for magnetic studies.[12f] All other reagents were used as purchased without further purification.

$\{K_7Na[Cu_4K_2(H_2O)_6(\alpha\text{-}AsW_9O_{33})_2]\cdot 5.5H_2O\}_n$ (K_7Na-1). A 0.51 g (3.0 mmol) sample of $CuCl_2\cdot 2H_2O$ was dissolved in 40 mL of

(9) Wassermann, K.; Dickman, M. H.; Pope, M. T. *Angew. Chem.* **1997**, *109*, 1513; *Angew. Chem., Int. Ed. Engl.* **1997**, *36*, 1445.

(10) (a) Tourné, C.; Revel, A.; Tourné, G.; Vendrell, M. *C. R. Acad. Sci., Ser. C* **1973**, *277*, 643. (b) Rosenheim, A.; Wolff, A. *Z. Anorg. Allg. Chem.* **1930**, *64*, 193. (c) Gibbs, W. *J. Am. Chem. Soc.* **1885**, *7*, 317.

(11) (a) Jeannin, Y.; Martin-Frère, J. *Inorg. Chem.* **1979**, *18*, 3010. (b) Jeannin, Y.; Martin-Frère, J. *J. Am. Chem. Soc.* **1981**, *103*, 1664. (c) Leyrie, M.; Tézé, A.; Hervé, G. *Inorg. Chem.* **1985**, *24*, 1275. (d) Jeannin, Y. *C. R. Acad. Sci., Ser. IIc* **2000**, *3*, 295. (e) Kortz, U.; Savelieff, M. G.; Bassil, B. S.; Dickman, M. H. *Angew. Chem.* **2001**, *113*, 3488; *Angew. Chem., Int. Ed.* **2001**, *40*, 3384.

(12) (a) Robert, F.; Leyrie, M.; Hervé, G.; Tézé, A.; Jeannin, Y. *Inorg. Chem.* **1980**, *19*, 1746. (b) Robert, F., Leyrie, M., Hervé, G. *Acta Crystallogr.* **1982**, *B38*, 358. (c) Weakley, T. J. R. *Inorg. Chim Acta* **1984**, *87*, 13. (d) Martin-Frère, J.; Jeannin, Y. *Inorg. Chem.* **1984**, *23*, 3394. (e) Sazani, G.; Dickman, M. H.; Pope, M. T. *Inorg. Chem.* **2000**, *39*, 939. (f) Kortz, U.; Al-Kassem, N. K.; Savelieff, M. G.; Al Kadi, N. A.; Sadakane, M. *Inorg. Chem.* **2001**, *40*, 4742. (g) Mialane, P.; Marrot, J.; Rivière, E.; Nebout, J.; Hervé, G. *Inorg. Chem.* **2001**, *40*, 44. (h) Mialane, P.; Marrot, J.; Mallard, A.; Hervé, G. *Inorg. Chim. Acta* **2002**, *328*, 81.

(13) (a) Pope, M. T.; Wei, X. Y.; Wassermann, K.; Dickman, M. H. *C. R. Acad. Sci., Ser. IIc* **1998**, *1*, 297. (b) Wassermann, K.; Pope, M. T. *Inorg. Chem.* **2001**, *40*, 2763. (c) Kim, K.-C.; Pope, M. T. *J. Chem. Soc., Dalton Trans.* **2001**, 986. (d) Kim, K.-C.; Gaunt, A.; Pope, M. T. *J. Cluster Sci.* **2002**, *13*, 423. (e) Fukaya, K.; Yamase, T. *Angew. Chem., Int. Ed.* **2003**, *42*, 654. (f) Kortz, U.; Holzapfel, C.; Reicke, M. *J. Mol. Struct.* **2003**, *656*, 93.

(14) (a) Siedle, A. R.; Padula, F.; Baranowski, J.; Goldstein, C.; DeAngelo, M.; Kokoszka, G. F.; Azevedo, L.; Venturini, E. L. *J. Am. Chem. Soc.* **1983**, *105*, 7447. (b) Kokoszka, G. F.; Padula, F.; Goldstein, A. S.; Venturini, E. L.; Azevedo, L.; Siedle, A. R. *Inorg. Chem.* **1988**, *27*, 59.

(15) Cho, Y. H.; So, H. *Bull. Korean Chem. Soc.* **1995**, *16*, 243.

Table 1. Crystal Data and Structure Refinement for K_7Na-**1**

empirical formula	$As_2Cu_4H_{23}K_9NaO_{77.5}W_{18}$	temp (°C)	−100
fw	5351.4	wavelength (Å)	0.71073
space group (No.)	$P\bar{4}2_1m$ (113)	d_{calcd} (Mg m^{-3})	4.544
a, b (Å)	16.705(4)	abs coeff (mm^{-1})	28.966
c (Å)	13.956(5)	R^a [$I > 2\sigma(I)$]	0.046
vol (Å^3)	3894.5(19)	$R_w{}^b$ (all data)	0.107
Z	2		

^{a} $R = \sum||F_o| - |F_c||/\sum|F_o|$. ^{b} $R_w = [\sum w(F_o^2 - F_c^2)^2/\sum w(F_o^2)^2]^{1/2}$.

H_2O, and then 4.0 g (1.5 mmol) of $K_9[\alpha\text{-}AsW_9O_{33}]$ was added. The solution was refluxed for 1 h and filtered after cooling. Slow evaporation at room temperature resulted in 2.9 g of a green, crystalline product which was isolated and air-dried (yield 73%). IR: 974(sh), 950(s), 907(s), 888(sh), 864(sh), 788(sh), 749(s), 736(s), 484(w), 465(w) cm^{-1}. Anal. Calcd (Found) for $\{K_7Na[Cu_4K_2(H_2O)_6(\alpha\text{-}AsW_9O_{33})_2]\cdot 5.5H_2O\}_n$: K, 6.6 (6.5); Na, 0.43 (0.37); W, 61.8 (61.4); Cu, 4.8 (4.9); As, 2.80 (2.67).

Elemental analysis was performed by Kanti Labs Ltd. in Mississauga, Canada. Infrared spectra were recorded on KBr pellets using a Nicolet Avatar spectrophotometer.

X-ray Crystallography. A green, block-shaped crystal with dimensions 0.04 × 0.08 × 0.10 mm^3 was mounted onto a glass fiber for indexing and intensity data collection on a Siemens SMART-CCD single-crystal diffractometer using Mo Kα radiation ($\lambda = 0.71073$ Å). Direct methods were used to solve the structure and to locate the tungsten atoms (SHELXS86). Then the remaining atoms were found from successive difference maps (SHELXL93). Routine Lorentz and polarization corrections were applied, and an absorption correction was performed using the SADABS program.[17] Crystallographic data are summarized in Table 1.

Magnetic Susceptibility Measurements. Magnetic susceptibility (χ) measurements of K_7**Na-1** and Na_9**-2** were carried out using a Quantum Design MPMS-XL SQUID magnetometer. Data for polycrystalline samples of K_7**Na-1** and Na_9**-2** were collected over 1.8−200 K at 1000 G, using 66.20 and 75.35 mg masses, respectively. The data were corrected for the sample holder, diamagnetism using Klemm constants,[18] and temperature-independent paramagnetism (TIP) contributions.

EPR Spectroscopy. Polycrystalline powder EPR spectra of K_7**Na-1** and Na_9**-2** were recorded using a Bruker Elexsys-500 spectrometer at the X-band (~9.5 GHz) and Q-band (~34 GHz) in the 4−300 K temperature range. Also, single-crystal EPR spectra of Na_9**-2** were recorded at the Q-band to gain more precise information on the magnetic parameters. W-band measurements were conducted at the high-field electron magnetic resonance facility at the National High Magnetic Field Laboratory in Tallahassee.[19] An Oxford Instruments Teslatron superconducting magnet sweepable between 0 and 17 T was used to apply the Zeeman field. In all experiments the modulation amplitudes and microwave power were adjusted for optimal signal intensity and resolution. All EPR spectra were simulated using Bruker's Simfonia and Xsophe programs.

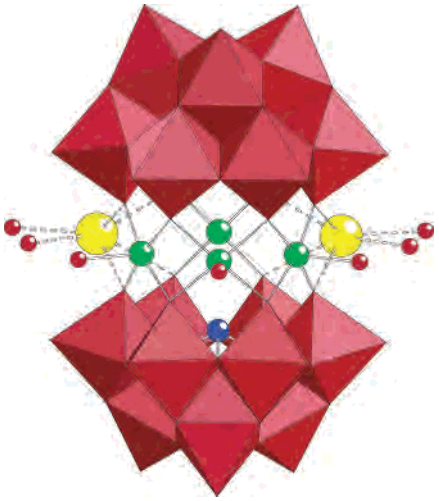

Figure 1. Combined polyhedral/ball-and-stick representation of **1**. The WO_6 octahedra are shown in red, and the balls represent copper (green), arsenic (blue), potassium (yellow), and water molecules (red).

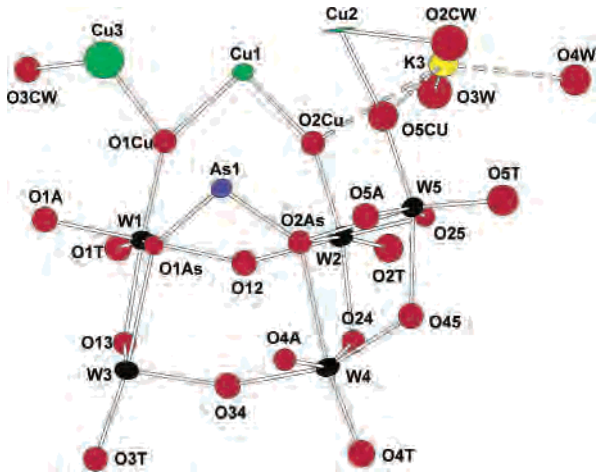

Figure 2. Ball-and-stick representation of the asymmetric unit of **1** showing 50% probability ellipsoids and the labeling scheme.

Results and Discussion

Synthesis and Structure. The dimeric polyoxoanion $[Cu_4K_2(H_2O)_8(\alpha\text{-}AsW_9O_{33})_2]^{8-}$ (**1**) consists of two $[\alpha\text{-}AsW_9O_{33}]^{9-}$ moieties linked by four Cu^{2+} and two K^+ ions, resulting in a sandwich-type structure with idealized C_{2v} symmetry (see Figures 1 and 2). The central belt of polyanion **1** is composed of three adjacent, edge-shared $CuO_4(H_2O)$ square pyramids and a unique $CuO_4(H_2O)$ fragment which is separated from the copper triad by two potassium ions (see Figure 3). This arrangement was somewhat unexpected because all other dimeric, sandwich-type tungstoarsenates(III) contain only two or three transition-metal ions in the central belt and the vacancies between them are usually occupied by sodium or potassium ions.[12f,g,16] The

(16) The presence of a sodium ion in $K_7Na[Cu_4K_2(H_2O)_8(\alpha\text{-}AsW_9O_{33})_2]\cdot 3.5H_2O$ (K_7**Na-1**) was confirmed by X-ray diffraction and elemental analysis. Most likely the sodium ion originates from a small impurity in our $K_9[\alpha\text{-}AsW_9O_{33}]$ precursor, which was obtained by the addition of solid KCl to a freshly synthesized aqueous solution of $Na_9[\alpha\text{-}AsW_9O_{33}]$. However, in the solid-state structure of K_7**Na-1** this sodium ion is not associated at all with oxygen atoms of **1**. It is located more than 5 Å away from the closest polyanion and is surrounded by six water molecules. Two of the water molecules (trans to each other) are terminal, and the other four are coordinated to potassium ions in the cationic/crystal water lattice. We are convinced that the sodium ion does not play any important role in the formation of **1**.

(17) Sheldrick, G. M. *SADABS*; Siemens Analytical X-ray Instrument Division: Madison, WI, 1995.

(18) Vulfson, S. G. *Molecular Magnetochemistry*; Gordon and Breach Science: Newark, NJ, 1998; p 241.

(19) (a) Cage, B.; Hassan, A. K.; Pardi, L.; Krzystek, J.; Brunel, L.-C.; Dalal, N. S. *J. Magn. Reson.* **1997**, *124*, 495. (b) Hassan, A. K.; Pardi, L. A.; Krzystek, J.; Sienkiewicz, A.; Goy, P.; Rohrer, M.; Brunel, L.-C. *J. Magn. Reson.* **2000**, *142*, 300.

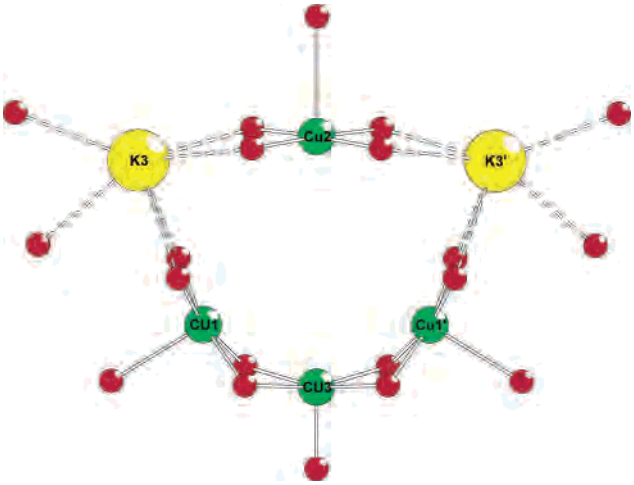

Figure 3. Ball-and-stick representation of the central belt in **1**. The color code is the same as in Figure 1.

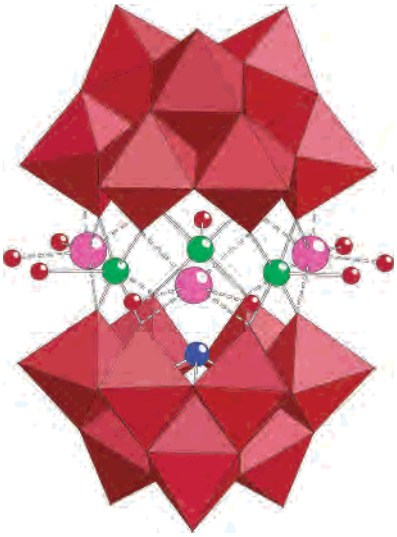

Figure 4. Combined polyhedral/ball-and-stick representation of **2**. The sodium atoms are shown in purple; otherwise the color code is the same as in Figure 1.

tricopper-substituted species $[Cu_3Na_3(H_2O)_9(\alpha\text{-}AsW_9O_{33})_2]^{9-}$ (**2**; see Figure 4) is most closely related to **1**. The latter is derived from the former by substitution of a sodium by a cupric ion. The structure of **1** is also in marked contrast to Hervé's $[Cu_3K_3(H_2O)_4(\alpha\text{-}AsW_9O_{33})_2]^{9-}$ (**1a**; see Figure 5), which was isolated as a potassium salt.[12b] They observed a dimeric, sandwich-type polyanion incorporating three copper ions which however were not equivalent. Only two of them had a terminal water molecule, resulting in square-pyramidal coordination, whereas the third Cu^{2+} ion exhibited square-planar coordination. The three incorporated potassium ions were also inequivalent, and interestingly, two K^+ ions had only one terminal water ligand whereas the third K^+ ion had no terminal ligand at all. Furthermore, the authors identified a glide of one AsW_9O_{33} subunit with respect to the other which they explained to be a result of lone-pair/lone-pair repulsion of the two As(III) atoms. The symmetry of the anion was reduced to C_s.

In our attempts to synthesize more copper-rich derivatives of polyanion **2**, we decided to react a mixed potassium/

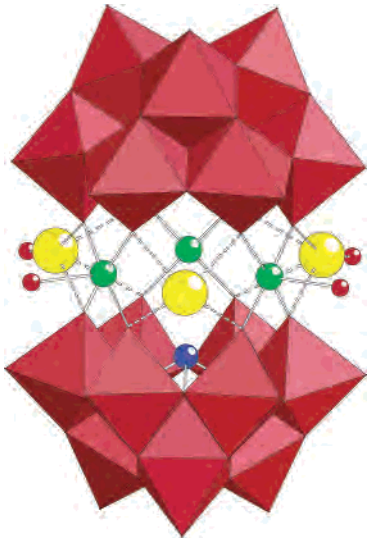

Figure 5. Combined polyhedral/ball-and-stick representation of **1a**. The color code is the same as in Figure 1.

sodium salt of $[\alpha\text{-}AsW_9O_{33}]^{9-}$ with Cu^{2+} ions in a 1:2 ratio in neutral, aqueous medium. We obtained $\mathbf{K_7Na}$**-1** in crystalline form and high yield. It is of interest to evaluate the conditions that favor formation of polyanions **1**, **2**, and **1a** in aqueous solution. We have observed previously that sodium ions play an important role in the stabilization of **2** in the solid state and most likely also in solution.[12f] The work of Hervé has shown that substitution of sodium by potassium ions has a subtle, but significant, effect on the polyanion structure.[12b] We have discovered that an excess of Cu^{2+} ions combined with a low concentration of sodium ions allows for incorporation of more than three copper ions in the dimeric tungstoarsenate(III) framework. Unfortunately, most analytical techniques do not allow the trisubstituted polyanion (**2**) to be unequivocally distinguished from the tetrasubstituted (**1**) or distorted trisubstituted (**1a**) polyanion in the solid state. On the basis of our observations, single-crystal XRD is the only reliable experimental method. However, even with this powerful technique, it is necessary to perform a complete data collection, because the unit cell parameters are not sufficient. We have collected several (unpublished) X-ray structures which were isomorphous, although in some cases three and in others four copper ions were present in the central section of the dimeric polyanion structure. Of course, elemental analysis must be used to confirm the XRD results.

The solid-state structure of $\mathbf{K_7Na}$**-1** is composed of individual polyoxoanions **1** that are connected to four neighbors via four Cu1−O3T−W3 bonds, leading to a 2D network (see Figures 6 and 7). The two equivalent copper centers Cu1 and Cu1′ of **1** are linked to the tungsten center W3 in a cap of each of the two adjacent polyanions. At the same time the two symmetrically equivalent tungsten centers W3 and W3′ in the two caps of **1** are covalently linked to the two equivalent copper centers Cu1 of each of the two additional, adjacent polyanions. This solid-state arrangement is clearly a result of the unsymmetrical distribution of the four copper ions within the belt of each polyanion **1**. Three of the four Cu^{2+} ions (Cu1, Cu1′, Cu3) are adjacent on the

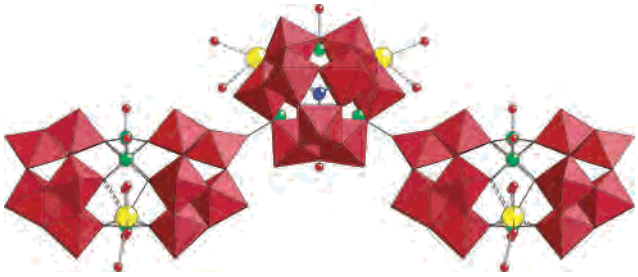

Figure 6. Combined polyhedral/ball-and-stick representation indicating the connectivities of neighboring polyanions via Cu1−O3T−W3 bridges in the lattice of **K_7Na-1**. The color code is the same as in Figure 1.

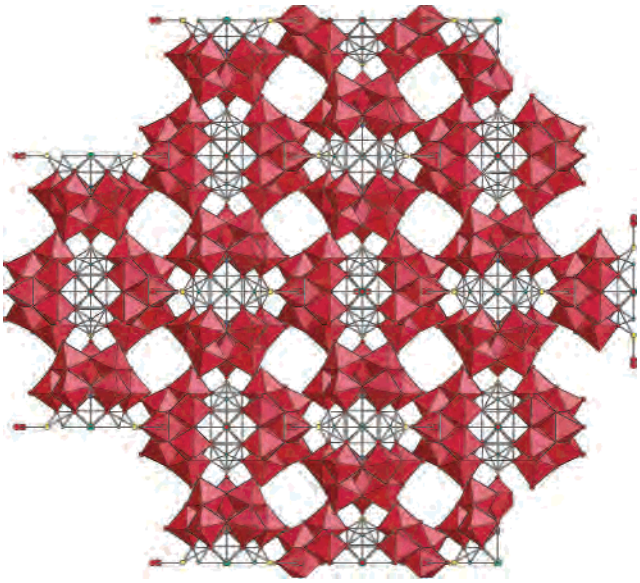

Figure 7. Combined polyhedral/ball-and-stick representation of the two-dimensional arrangement of **K_7Na-1**. The color code is the same as in Figure 1.

"copper-rich" side of the ring, whereas the remaining Cu2 is located on the "copper-poor" side of the ring (separated from each other by the two equivalent potassium ions K3 and K3′). The lattice of **K_7Na-1** can be described as double layers of **1** where the copper-rich sections of the central belt point at each other. However, the polyanions in one layer are arranged vertically, whereas the polyanions in the other layer are arranged horizontally, and all polyanions in the "vertical layer" are completely offset with respect to those in the "horizontal layer" (see Figure 7). We expect that almost certainly the interpolyanion connectivities are broken after redissolution of the crystalline salt in water, resulting in the presence of discrete polyanions where all copper centers have terminal H_2O ligands. This is supported by the observation that the W3−O3T (1.725(19) Å) and Cu1−O3T (2.308(19) Å) bonds both have terminal character, indicating very weak interaction between neighboring polyanions in the solid state.

It is of interest to investigate all bond lengths and angles within the central section of **1**, especially for the three adjacent copper ions (see Figure 3). The square-pyramidal coordination spheres of Cu1 (Cu1−O_{eq}, 1.909−1.929(14) Å; Cu1−O_{ax}, 2.308(19) Å) and Cu2 (Cu2−O_{eq}, 1.953(15) Å; Cu2−O_{ax}, 2.553(20) Å) are fairly regular and exhibit the expected Jahn−Teller distortion (axial elongation), which has already been observed for **Na_9-2**.[12f] It is not unexpected that also Cu3 exhibits a Jahn−Teller distortion, but interestingly, it is an axial compression (Cu3−O_{eq}, 2.020(14) Å; Cu3−O_{ax}, 1.76(3) Å). This is rather unusual and is obviously a result of the inflexible nature of the four symmetry-equivalent O1Cu atoms spanning the equatorial plane for Cu3. These oxygen atoms are rather fixed because they belong to the backbone of **1**, which is composed of two AsW_9O_{33} fragments and the three copper centers Cu1, Cu1′, and Cu2. Therefore, the Cu3 atom encounters a coordination environment that necessarily results in long equatorial Cu3−O bonds, but this is compensated by a tetragonal distortion, leading to a very short axial Cu−OH_2 bond. As a result the unpaired electron of Cu3 is expected to occupy the d_{z2} orbital, whereas the unpaired electron of each of the neighboring Cu1 and Cu1′ atoms is expected to be in the respective d_{x2-y2} orbital. To our knowledge, **1** represents the first copper(II)-containing polyoxoanion with both forms of tetragonal distortion (axial elongation and compression) being present.

The equatorial bond angles around the copper ions Cu1 (O−Cu1−O, 85.3−91.3(7)°) and Cu2 (O−Cu2−O, 89.5−90.4(10)°) are very regular and also similar to those of **Na_9-2**.[12f] On the other hand, the bond angles around the copper ion Cu3 (O−Cu3−O, 80.6−97.7(8)°) are more irregular, so its coordination geometry is best described as rectangular pyramidal (see Figure 3). The three copper ions Cu1, Cu3, and Cu1′ represent a very interesting and unique spin system connected via μ_2-oxo ligands. Furthermore, the Cu1···Cu3 distance is only 2.766(5) Å, so we decided to perform a detailed investigation of the magnetic properties of **1** including EPR. Interestingly, the separations of the two arsenic atoms in polyanions **1** and **1a** are very similar (5.34 vs 5.33 Å).

It can be noticed in Figure 2 that Cu2 exhibits a rather elongated thermal ellipsoid more or less along the Cu2−OH_2 bond. This is a result of the disorder over three positions that are very close to each other (<0.5 Å). We were able to account for all significant electron density by anisotropic refinement of Cu2 (largest difference peak and hole 2.899 and −3.434 e Å^{-3}). The partial occupancy model was not used because the disorder is very uneven, with the central position accounting for more than 90% of the electron density. The Cu2 atom is bound to the terminal water molecule O2CW, which is evenly disordered over two positions.

In addition to the four copper(II) ions, polyanion **1** also incorporates two K^+ ions within the central belt. The potassium ions K3 and K3′ are located in cavities separating the copper ions Cu1, Cu2, and Cu1′ and are bound to four oxygen atoms of the two AsW_9O_{33} fragments and two terminal water molecules (see Figures 1−3). The potassium−oxygen bond lengths of the two incorporated potassium ions are within the expected ranges (K3···O, 2.824−2.839(16) Å; K3···OH_2, 2.81−2.82(3) Å), and therefore, the potassium ions are drawn into the polyoxoanion framework much less than the sodium ions in **2** (Na1···O, 2.456−2.480(7) Å; Na2···OH_2, 2.339(7)−2.494(7) Å; see also Figure 4).[12f] We

Chart 1

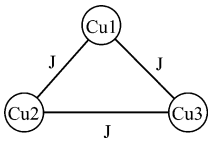

have already pointed out the stabilizing role of the three incorporated sodium ions for the dimeric tungstoarsenate-(III), which resulted in facile synthesis and isolation of **2** as a crystalline product in very high yield and over a large pH range (3−8).[12f] We believe that the low stability of the hypothetical tri-potassium-incorporated species $[Cu_3K_3(H_2O)_9(\alpha\text{-}AsW_9O_{33})_2]^{9-}$ (**1b**) is indicated by (a) isolation of Hervé's distorted polyanion **1a** and (b) isolation of **1**, which seems to be formed more easily than **1b**. Interestingly, **1** also seems to be formed more easily than **1a** (at least in our hands).

Magnetic Studies. Magnetic Susceptibility. The Hamiltonian for a system containing a cluster of exchange-coupled ions, in the presence of an external field **H**, is given by eq 1.

$$\mathscr{H} = -2\sum_{i\neq j} J_{ij} S_i \cdot S_j + \beta \mathbf{H}\cdot\mathbf{g}\cdot\sum_i S_i \qquad (1)$$

Here J_{ij} is the isotropic spin exchange constant, S_i is the spin operator of the ith ion, β is the electronic Bohr magneton, and **g** is the Landé **g** tensor. For the susceptibility analysis we neglected the hyperfine interactions with the ^{63,65}Cu nuclei, because they were not resolved in our EPR spectra, likely because the rate of the spin exchange process is higher than the hyperfine splitting. Also neglected are the zero-field splitting terms D and E, since they were much smaller than J, as verified by EPR measurements (vide infra). Substitution of the eigenvalues of eq 1 into the standard Van Vleck equation yields the expression for the molar magnetic susceptibility (χ_m), as shown in eq 2.[20]

$$\chi_m = \left(\frac{Ng^2\beta^2}{3k(T-\Theta)}\right)\left(\frac{\sum_n S_n{}^T(S_n{}^T+1)(2S_n{}^T+1)\exp(-E_n/kT)}{\sum_n (2S_n{}^T+1)\exp(-E_n/kT)}\right) \qquad (2)$$

Here, N is the Avogadro number, k the Boltzmann constant, T the temperature in Kelvin, Θ the Weiss constant, and E_n the spin exchange energy associated with a spin state $S_n{}^T$. The observed magnetic data of compounds $\mathbf{K_7Na}$**-1** and $\mathbf{Na_9}$**-2** were analyzed using eq 2 as outlined below.

(a) Theoretical Model and Susceptibility Data for $(Cu^{2+})_3$ of Na_9-2. Polyanion **2** has three Cu^{2+} ions arranged in a triangular fashion as shown in Chart 1 with Cu−Cu distances $Cu_1-Cu_2 = Cu_1-Cu_3 = 4.696$ Å and $Cu_2-Cu_3 = 4.689$ Å.[12f] Since the possible superexchange paths between any two Cu^{2+} ions of polyanion **2** are the same (Cu−O−W−O−W−O−Cu), for our analysis we assume the Cu−Cu distances to be equal and hence the Cu_3 system to be an equilateral triangle. For Cu_3 here, eq 1 becomes

$$\mathscr{H} = -2J[S_1\cdot S_2 + S_2\cdot S_3 + S_1\cdot S_3] \qquad (3)$$

Following Kambe,[21] we define $S_{23} = S_2 + S_3$ and $S^T = S_1 + S_{23}$. Then eq 3 can be rearranged as

$$\mathscr{H} = -J[(S^T)^2 - (S_1)^2 - (S_2)^2 - (S_3)^2] \qquad (4)$$

with eigenvalues

$$E(S^T,S_1,S_2,S_3) = -J[S^T(S^T+1) - S_1(S_1+1) - S_2(S_2+1) - S_3(S_3+1)] \qquad (5)$$

For each Cu^{2+} ion, since $S_1 = S_2 = S_3 = 1/2$, eq 5 transforms into eq 6. Here S^T takes the values 1/2 (↑↑↓), 1/2 (↑↓↑) or 3/2 (↑↑↑),

$$E(S^T) = -J[S^T(S^T+1) - 9/4] \qquad (6)$$

with energies $3J/2$, $3J/2$, and $-3J/2$, respectively. The molar magnetic susceptibility (χ_m) for this system is then obtained by expanding eq 2 for all these spin states. This is as given in eq 7, in agreement with earlier studies.[20,22]

$$\chi_m = \frac{Ng^2\beta^2}{4k(T-\Theta)}\left[\frac{1+5\exp(3J/kT)}{1+\exp(3J/kT)}\right] \qquad (7)$$

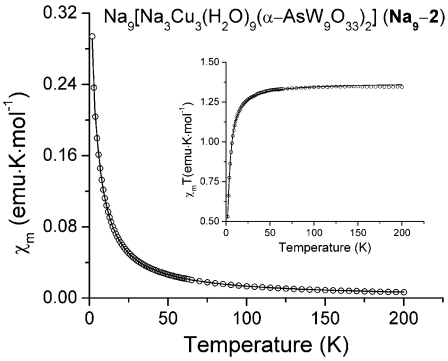

Figure 8. Temperature dependence of χ_m for $\mathbf{Na_9}$**-2** at $\mathbf{H} = 1000$ G. The inset displays the $\chi_m T$ vs T plot for $\mathbf{Na_9}$**-2**. Open circles represent the experimental data, and the solid line represents the theoretical curve (see the text).

Figure 8 shows the measured temperature dependence of χ_m for $\mathbf{Na_9}$**-2**. It is seen that χ_m remains almost constant at about 0.02 emu·mol^{-1} down to 60 K and then steadily increases to ∼0.3 emu·mol^{-1} at 1.8 K. A graph of $\chi_m T$ vs T over 1.8−200 K is shown in the inset. The nearly constant $\chi_m T$ value (∼1.34 emu·K·mol^{-1}) in the temperature region 60−200 K is indicative of the admixture of both $S^T = 1/2$ and $S^T = 3/2$ spin states. The experimental χ_m and $\chi_m T$ data have been fitted to eq 7 by treating J, g, and Θ as adjustable parameters. The agreement between the theoretical curve (solid line in Figure 8) and measured data is quite satisfac-

(20) Kahn, O. *Molecular Magnetism*; VCH: New York, 1993.

(21) Kambe, K. *J. Phys. Soc. Jpn.* **1950**, *5*, 48.

(22) (a) Clérac, R.; Cotton, F. A.; Dunbar, K. R.; Hillard, E. A.; Petrukhina, M. A.; Smucker, B. W. *C. R. Acad. Sci., Ser. IIc* **2001**, *4*, 315. (b) Cage, B.; Cotton, F. A.; Dalal, N. S.; Hillard, E. A.; Rakvin, B.; Ramsey, C. M. *J. Am. Chem. Soc.* **2003**, *125*, 5270.

Chart 2

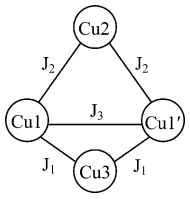

tory. The best least-squares fit is achieved with $J = -1.36 \pm 0.01$ cm^{-1} (-1.96 ± 0.01 K), $g_{iso} = 2.208 \pm 0.001$, and $\Theta = -0.026 \pm 0.001$ cm^{-1} (-0.037 ± 0.001 K). This is consistent with $g_{iso} = 2.208 \pm 0.001$ obtained directly from EPR measurements (vide infra). The small magnitude of Θ shows that the intercluster interactions in polyanion **2** are negligible.

In **2** the Cu $3d_{x2-y2}$ orbitals, which contain the unpaired electrons, are directed along the Cu$-$O$_{eq}$ vectors. Therefore, stabilization of the $S^T = 1/2$ and $S^T = 3/2$ spin states must involve indirect electronic coupling pathways. The available indirect pathway for the magnetic exchange interaction in **2** is via six bonds involving two tungsten and three oxygen atoms of each AsW_9O_{33} fragment. Hence, we expect the interaction between the Cu^{2+} ions to be very weak. This is supported by the small magnitude of the spin exchange coupling constant $J \approx -1$ cm^{-1}. The negative sign of J indicates the presence of antiferromagnetic intratrimer coupling between the three Cu^{2+} ions of **2**. As can be noted from Figure 7, the lowest value of $\chi_m T$ was 0.53 emu·K·mol^{-1}. Thus, while we were unable to attain low enough temperature to ascertain the expected $\chi_m T$ value of 0.457 emu·K·mol^{-1} corresponding to $g_{iso} = 2.208$ for the $S^T = 1/2$ state in the $\chi_m T$ vs T plots of **Na$_9$-2**, our conclusion is considered fairly definitive.

(b) Theoretical Model and Susceptibility Data for $(Cu^{2+})_4$ of K$_7$Na-1. The four Cu^{2+} ions of **1** are arranged in a distorted rhombus as shown in Chart 2 with Cu$-$Cu distances $Cu_3-Cu_1 = Cu_3-Cu_{1'} = 2.766$ Å, $Cu_1-Cu_{1'} = 4.835$ Å, and $Cu_2-Cu_1 = Cu_2-Cu_{1'} = 4.734$ Å. This system can be described in terms of the three exchange constants J_1, J_2, and J_3 as shown in Chart 2. The exchange constant between Cu_2 and Cu_3 is set equal to zero because of the large distance (5.42 Å or eight bonds).

For polyanion **1** the expanded spin exchange Hamiltonian has the form shown in eq 8 with the spin exchange coupling constants J_1, J_2, and J_3 as indicated above.

$$\mathscr{H} = -2J_1[S_3\cdot S_1 + S_3\cdot S_{1'}] - 2J_2[S_2\cdot S_1 + S_2\cdot S_{1'}] - 2J_3[S_1\cdot S_{1'}] \quad (8)$$

By defining $S_{11'} = S_1 + S_{1'}$, $S_{23} = S_2 + S_3$, $S_{311'} = S_3 + S_{11'}$, and $S^T = S_2 + S_{311'}$ and following the vector-coupling method,[21] the eigenvalues of the Hamiltonian in eq 8 are found as follows:

$$E(S^T,S_{11'},S_{23},S_{311'},S_1,S_3,S_{1'}) = -J_1[S_{311'}(S_{311'}+1) - S_{11'}(S_{11}+1) - S_3(S_3+1)] - J_2[S^T(S^T+1) - S_{311'}(S_{311'}+1) - S_{23}(S_{23}+1) + S_3(S_3+1)] - J_3[S_{11'}(S_{11'}+1) - S_1(S_1+1) - S_{1'}(S_{1'}+1)] \quad (9)$$

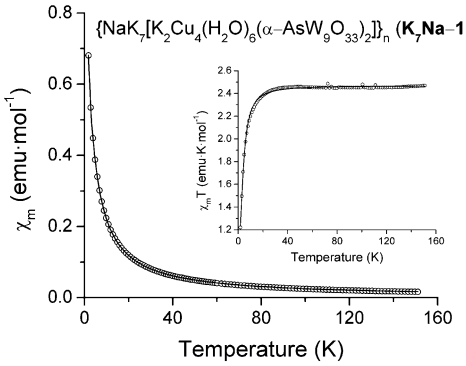

Figure 9. χ_m vs T plot of **K$_7$Na-1** at **H** = 1000 G. The inset shows the temperature dependence of $\chi_m T$ for **K$_7$Na-1**. The open circles represent the experimental data, and the solid line represents the theoretical curve (see the text).

Table 2. Allowed Spin States and Their Energies of the $(Cu^{2+})_4$ Tetrad in **1**, Using Eq 10 in the Text

state i	S_{23}	$S_{11'}$	$S_{311'}$	S^T	$E_i(S^T,S_{11'},S_{23},S_{311'})$
1	0	0	1/2	0	$3J_3/2$
2	0	0	1/2	1	$-2J_2 + 3J_3/2$
3	0	1	1/2	0	$2J_1 - J_3/2$
4	0	1	1/2	1	$2J_1 - 2J_2 - J_3/2$
5	0	1	3/2	1	$-J_1 + J_2 - J_3/2$
6	0	1	3/2	2	$-J_1 - 3J_2 - J_3/2$
7	1	0	1/2	0	$2J_2 + 3J_3/2$
8	1	0	1/2	1	$3J_3/2$
9	1	1	1/2	0	$2J_1 + 2J_2 - J_3/2$
10	1	1	1/2	1	$2J_1 - J_3/2$
11	1	1	3/2	1	$-J_1 + 3J_2 - J_3/2$
12	1	1	3/2	2	$-J_1 - J_2 - J_3/2$

For each Cu^{2+} ion $S_1 = S_2 = S_3 = S_{1'} = 1/2$, so both $S_{11'}$ and S_{23} can take the values of 0 and 1 and eq 9 takes the form

$$E(S^T,S_{11'},S_{23},S_{311'}) = -J_1[S_{311'}(S_{311'}+1) - S_{11'}(S_{11'}+1) - 3/4] - J_2[S^T(S^T+1) - S_{311'}(S_{311'}+1) - S_{23}(S_{23}+1) + 3/4] - J_3[S_{11'}(S_{11'}+1) - 3/2] \quad (10)$$

The allowed values of $S_{11'}$, S_{23}, $S_{311'}$, S^T and the corresponding eigenvalues, as given by eq 10, are presented in Table 2. The molar magnetic susceptibility (χ_m) for this $(Cu^{2+})_4$ tetrad is then obtained by substituting the energies of Table 2 into eq 2, as given below:

$$\chi_m = \left(\frac{2Ng^2\beta^2}{k(T-\Theta)}\right)\left(\frac{A}{B}\right) \quad (11)$$

where $A = \exp(2x + 5y) + \exp(5y + 2z) + \exp(2x + 3y) + \exp(3y + 2z) + \exp(3x + 2z) + \exp(3x + 2y + 2z) + 5\exp(3x + 6y + 2z) + 5\exp(3x + 4y + 2z)$ and $B = \exp(2x + y) + \exp(y + 2z) + 3\exp(2x + 5y) + 3\exp(5y + 2z) + 4\exp(2x + 3y) + 4\exp(3y + 2z) + 3\exp(3x + 2z) + 3\exp(3x + 2y + 2z) + 5\exp(3x + 6y + 2z) + 5\exp(3x + 4y + 2z)$ with $x = J_1/kT$, $y = J_2/kT$, and $z = J_3/kT$.

Figure 9 shows a plot of χ_m vs T for **K$_7$Na-1**. It is seen that χ_m slowly increases from about 0.02 emu·mol^{-1} at 150 K to ~0.04 emu·mol^{-1} at 60 K and then exponentially to ~0.7 emu·mol^{-1} at 1.8 K. The inset shows a plot of $\chi_m T$ vs T over the same temperature region. The almost constant $\chi_m T$ value of ~2.45 emu·K·mol^{-1} in the 60$-$150 K region

indicates the joint role of both $S^T = 1$ and $S^T = 2$ spin states, as discussed in the following section. The fitted curve is shown as the solid line in Figure 9. The agreement is again considered satisfactory. The best-fit parameters are $g_{iso} = 2.566 \pm 0.001$, $J_1 = 2.78 \pm 0.13$ cm^{-1} (3.99 ± 0.19 K), $J_2 = -1.35 \pm 0.02$ cm^{-1} (-1.95 ± 0.03 K), $J_3 = -2.24 \pm 0.06$ cm^{-1} (-3.23 ± 0.09 K), and $\Theta = -0.072 \pm 0.001$ cm^{-1} (-0.104 ± 0.002 K). The g_{iso} of 2.566 and the g_{iso} of 2.440 from EPR measurements (vide infra) agree with each other within experimental error. Again, the small magnitude of Θ indicates the presence of very weak intercluster interactions. Note that the magnitudes of all J values are comparable, so the Cu_4 moiety in **1** is a frustrated system with many low-lying excited states.

Although there is a possibility of a weak bond between Cu_3 and $Cu_{1(1')}$ (Cu_3–$Cu_{1(1')} = 2.766$ Å), only indirect pathways are available for electronic coupling between Cu^{2+} ions of **1**. The reason is that the orbitals bearing the unpaired electrons ($3d_{x2-y2}$ for $Cu_{1(1')}$ and Cu_2 and $3d_{z2}$ for Cu_3) are directed along the $Cu-O_{eq(ax)}$ vectors. The magnetic susceptibility measurements of **K_7Na-1** indicate the presence of both ferromagnetic and antiferromagnetic interactions in the $(Cu^{2+})_4$ tetrad, the latter being dominant. The observed magnitudes and signs of the exchange parameters J_1, J_3, and J_2 (~ 3, ~ -2, and ~ -1 cm^{-1}, respectively) can be correlated to the arrangement of the four Cu^{2+} ions in **1** in the following way.

Cu_3 is bonded to Cu_1 and $Cu_{1'}$ through two bonds involving an oxygen atom of the AsW_9O_{33} fragment with a $Cu_{1'}-O-Cu_3$ ($Cu_{1'}-O-Cu_3$) bond angle of 88.9°. Hence, as predicted[23] the exchange coupling constant J_1 (~ 3 cm^{-1}) is positive and has a larger magnitude in comparison to J_3 and J_2. Since Cu_1 and $Cu_{1'}$ are coupled through four bonds involving Cu_3 and two oxygen atoms of each AsW_9O_{33} fragment, $|J_3| < |J_1|$. J_2 has a smaller magnitude than J_1 and J_3 as Cu_2 is coupled to Cu_1 and $Cu_{1'}$ via six bonds involving two tungsten and three oxygen atoms of each AsW_9O_{33} unit. The presence of overall antiferromagnetic interactions in the $(Cu^{2+})_4$ tetrad of **1** indicates that the ground-state spin can be either 0 or 1. We were unable to attain low enough temperatures to ascertain the ground spin state due to very small and similar exchange coupling constants.

To predict the ground state, we plotted the energy (given by eq 10) as a function of various J values. Figure 10a shows a plot of E_i/J_1 as a function of J_3/J_1 at a fixed value of $J_2/J_1 = -0.5$, while Figure 10b shows a plot of E_i/J_1 as a function of J_2/J_1 at a fixed value of $J_3/J_1 = -0.75$. Both of these plots indicate that for ratios $J_3/J_1 = -0.75$ and $J_2/J_1 = -0.5$ the ground spin state of the $(Cu^{2+})_4$ tetrad is a mixture of both triplet ($S^T = 1$) and singlet ($S^T = 0$) states. Clearly, the $S^T = 1$ state results from spin frustration. This phenomenon has been observed previously for other copper, manganese, and iron clusters.[24,25]

EPR Spectroscopy. Additional verification of the disposition of the various spin−spin interactions, and also the zero-field splitting D, was obtained through EPR measurements as discussed below. EPR spectra of both **K_7Na-1** and **Na_9-2** were analyzed using the spin Hamiltonian shown in eq 12.

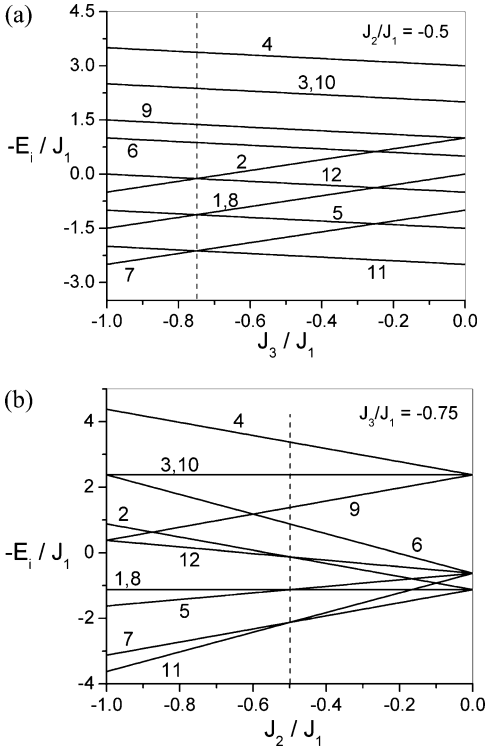

Figure 10. E_i/J_1 of the 12 spin states of **1** as a function of (a) J_3/J_1 at a fixed value of $J_2/J_1 = -0.5$ and (b) J_2/J_1 at a fixed value of $J_3/J_1 = -0.75$. The vertical dashed lines correspond to the experimental values of J_3/J_1 and J_2/J_1, respectively. Table 2 should be consulted to identify the 12 states.

$$\mathscr{H} = S^T \cdot D \cdot S^T + \beta H \cdot g \cdot S^T \qquad (12)$$

Here S^T is the total spin operator, D is the zero-field splitting parameter, and **g**, β, and **H** were defined earlier. The possible spin states correspond to a total spin $S^T = 3/2$ or 1/2 for **2** and 0, 1, or 2 for **1**. Here we neglect the hyperfine structure due to the $Cu^{63,65}$ nuclei, since it is exchange-averaged as mentioned earlier. Also, we do not consider J here because the variable-frequency EPR analysis shows no other effects that could be related to the exchange interaction. Assuming axial symmetry, and the high-field limit ($\mathbf{g}\beta\mathbf{H} \gg D$, as is the case here), the solution of eq 12 is straightforward.[26] The line centers will be given by the g factor, and each line will be split into $2S^T$ components. For $S^T = 1/2$ and $D = 0$, the spectral positions will be given by

$$h\nu = (g_{||}^2\beta^2H_{||}^2\cos^2\theta + g_{\perp}^2\beta^2H_{\perp}^2\sin^2\theta)^{1/2} \qquad (13)$$

where θ is the angle between the magnetic field and the axis of symmetry. For $S^T \geq 1$, each of the peaks will be split into $2S^T$ components by the **D** tensor, the splitting varying as

(23) Hodgson, D. J. *Prog. Inorg. Chem.* **1975**, *19*, 173.
(24) Gómez-Garcia, C. J.; Coronado, E.; Borrás-Almenar, J. J. *Inorg. Chem.* **1992**, *31*, 1667.
(25) McCuster, J. K.; Schmitt, E. A.; Hendrickson, D. N. In *Magnetic Molecular Materials*; Gatteschi, D., Kahn, O., Miller, J., Palacio, F., Eds.; NATO ASI Series; Kluwer Academic Publishers: Dordrecht, The Netherlands, 1991; Vol. 198.
(26) Abragam, A.; Bleaney, B. *Electron Paramagnetic Resonance of Transition Ions*; Dover Publications: New York, 1970.

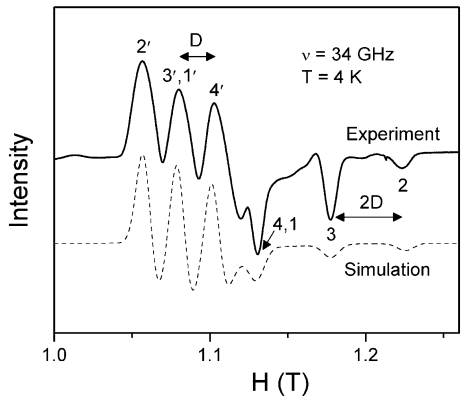

Figure 11. Experimental and simulated Q-band (34 GHz) powder EPR spectra of **Na**$_9$**-2** at 4 K. The numbers 2, 3, and 4 represent parallel peaks, while the numbers 2′, 3′, and 4′ represent perpendicular peaks, and the numbering refers to Figure 13b.

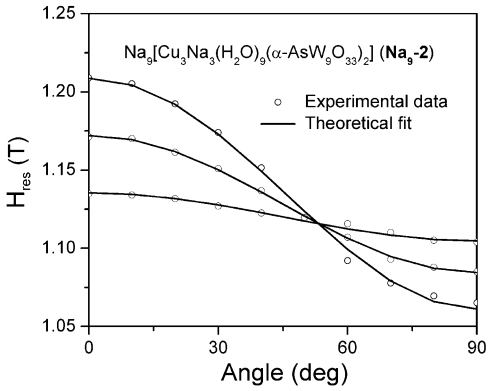

Figure 12. Comparison of the experimental angular dependence of **Na**$_9$**-2** with theory for the $S^T = 3/2$ state. The solid lines represent the calculated line positions, and the circles are experimental data from the Q-band EPR spectra at 4 K.

$$D(3\cos^2\theta - 1) \qquad (14)$$

Thus, for an $S^T = 3/2$ state and a powder pattern for $\mathbf{g}\beta\mathbf{H} \gg D$ the spectrum should consist of a triplet around $g_{||}$ and another at $g_\perp$, the triplet separation being $2D$ on the $g_{||}$ peak and D on the $g_\perp$ peak.

Figure 11 shows the experimental and simulated Q-band (34 GHz) powder EPR spectrum of **Na**$_9$**-2** at 4 K. The spectrum is characteristic of a quartet state corresponding to $S^T = 3/2$. The peak assignment is made using the energy level diagram shown in Figure 13b. We note that the Zeeman transitions of the $S^T = 1/2$ state (labeled 1 and 1′) are superimposed with peaks from the $S^T = 3/2$ state. In conformity with eq 14, for $S^T = 3/2$, we observe three transitions, labeled 2, 3, and 4 on the $g_{||} = 2.060 \pm 0.005$ component and 2′, 3′, and 4′ on the $g_\perp = 2.243 \pm 0.005$ component. Indeed, the triplet splitting is $2D$ for $g_{||}$ and $|D| = 230 \pm 5$ G (0.023 ± 0.005 cm^{-1}) for $g_\perp$. These data are listed in Table 3. The geometrical arrangement of CuO_4 groups in polyanion **2** is such that their perpendicular directions agree with the C_3 axis of the heteropolyanion while the parallel directions are perpendicular to the C_3 axis. If $\mathbf{g}(m)$ represents the **g** matrix for a CuO_4 group and **g** in eq 12 represents the molecular **g** matrix, assuming each Cu^{2+} ion has the same $g_{||}(m)$ and $g_\perp(m)$ values, the relation between them can be written[14a,15] as $g_{||} = g_\perp(m)$ and $g_\perp = [g_{||}(m) + g_\perp(m)]/2$. $g_{||}(m)$ and $g_\perp(m)$ values can then be calculated as 2.426 and 2.060, respectively, using the above-mentioned $g_{||}$ and $g_\perp$ values. The $g_{||}(m) > g_\perp(m) > g_e$ pattern proves that the unpaired electron resides in the d_{x2-y2} orbital.

In our single-crystal EPR experiments of **Na**$_9$**-2** at the Q-band, the crystal *c*-axis was aligned 10° with respect to the applied field direction to get maximum separation between the three fine structure peaks. X-ray diffraction studies[12f] confirm that this direction is the molecular C_3 axis. The angular dependence of the $S^T = 3/2$ state transitions as a function of crystal orientation relative to the applied magnetic field (**H**) was carried out at 4 K. The resulting resonance field positions were then simulated by employing a full-matrix diagonalization method of each of the fine structure transitions of the $S^T = 3/2$ state at each angle (θ) over the range 0−90°. Experimentally determined spin-Hamiltonian parameters (tabulated in Table 3) were used in the simulation. Figure 12 provides a comparison of the theoretical (solid curves) and experimental (open circles) resonance fields of the quartet state transitions with respect to the angle. At an angle $\theta = 55 \pm 5°$ the three resonance lines collapse to one based roughly on the $3\cos^2\theta - 1$ dependence of the zero-field splitting. The agreement between experimental and calculated line positions is considered to be satisfactory.

When the applied frequency is increased to the W-band (~95 GHz), the **g** tensor components further separate, providing more resolution and hence more information about the magnetic system. Because of weak spin exchange interaction, even at 4 K (Figure 13a), the Zeeman transitions arising from both the $S^T = 1/2$ and $S^T = 3/2$ states are observed. Zeeman transitions between the spin multiplets of 1/2 and 3/2 are not observed as they are forbidden.[26] While the parallel component of the $S^T = 1/2$ Zeeman transition is well resolved, the perpendicular component falls partially under the first perpendicular fine structure line of the quartet state. The spin Hamiltonian parameters of the $S^T = 1/2$ state are, therefore, $g_{||} = 2.117$ and $g_\perp = 2.254$. Simulation of the 4 K EPR spectrum with the experimental spin Hamiltonian parameters (lower panel of Figure 13a) is considered to be

Table 3. Spin Hamiltonian Parameters for Compounds **K**$_7$**Na-1** and **Na**$_9$**-2** from EPR and Magnetic Susceptibility Measurements

	EPR				magnetic susceptibility	
compd	S^T	$g_{||}$	$g_\perp$	$\|D\|$ (cm^{-1})	g_{iso}	J (cm^{-1})
K$_7$**Na-1**	1	2.221 ± 0.005	2.550 ± 0.005	0.073 ± 0.005	2.566 ± 0.001	$J_1 = 2.78 \pm 0.13$
	2	2.089 ± 0.005	2.210 ± 0.005	0.016 ± 0.005		$J_2 = -1.35 \pm 0.02$
						$J_3 = -2.24 \pm 0.06$
Na$_9$**-2**	1/2	2.117 ± 0.005	2.254 ± 0.005		2.208 ± 0.001	-1.36 ± 0.01
	3/2	2.060 ± 0.005	2.243 ± 0.005	0.023 ± 0.005		

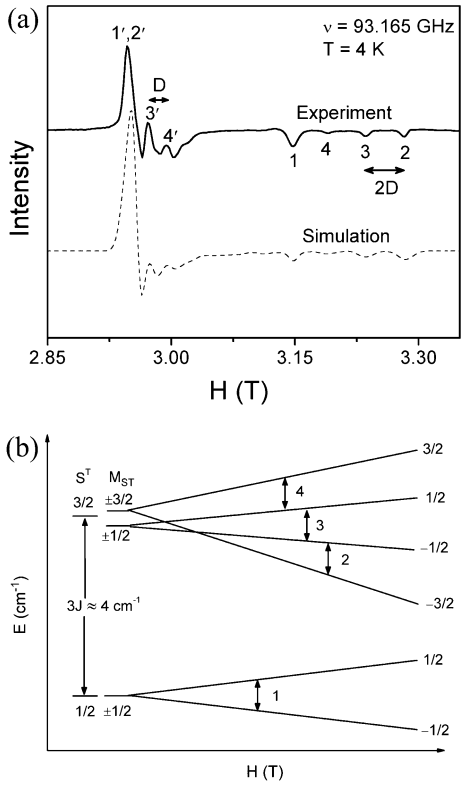

Figure 13. (a) Experimental and simulated W-band (ν = 93.165 GHz) powder EPR spectra of $\mathbf{Na_9}$**-2** at 4 K. (b) Energy level diagram and the expected EPR transitions.

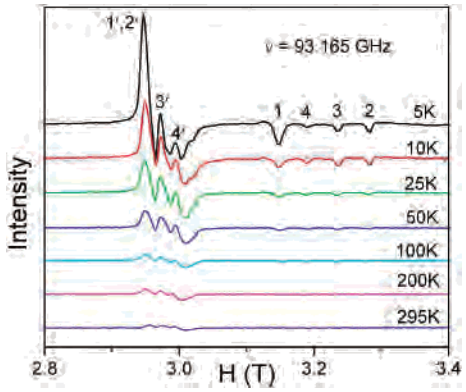

Figure 14. Temperature dependence of the W-band (ν = 93.165 GHz) EPR spectrum of $\mathbf{Na_9}$-2.

quite satisfactory. The temperature dependence of the W-band spectrum is shown in Figure 14. As the temperature is lowered, the parallel peak centered at 2.117 grows in intensity, thus confirming that the doublet spin state is in fact the ground state. At 4 K the fine structure line intensity shifts into the outermost parallel and perpendicular peaks, indicating a positive sign for the D value, and therefore that $M_S{}^T = \pm 1/2$ is the lower energy state.

As discussed earlier, the presence of a fourth Cu^{2+} ion in **1** changes the possible spin states, S^T, to 0, 1, and 2. Variable-temperature EPR spectra of $\mathbf{K_7Na}$**-1** were collected at the X-band (see Figure 15) to check if the compressed distortion at its Cu_3 site is a result of a dynamic Jahn−Teller effect.[27] Analysis of these EPR spectra shows that there is no change in the EPR line positions over the temperature range 4−300

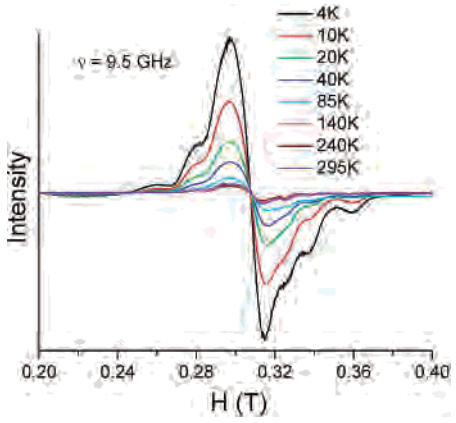

Figure 15. Variable-temperature EPR spectra of $\mathbf{K_7Na}$**-1** at the X-band (9.5 GHz).

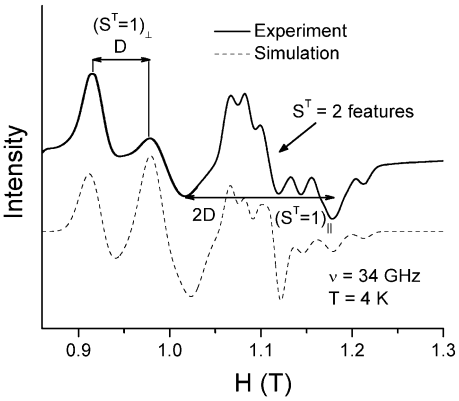

Figure 16. Experimental and simulated Q-band (34 GHz) powder EPR spectra of $\mathbf{K_7Na}$**-1** at 4 K.

K. The compressed distortion can therefore be considered as due to a static Jahn−Teller effect. Figure 16 shows the 34 GHz powder EPR spectrum of $\mathbf{K_7Na}$**-1** at 4 K. The spectrum can be analyzed as a superposition of $S^T = 2$ and $S^T = 1$ spin states, and the analysis outlined in eqs 13 and 14 is applicable here as well. The axial quartet pattern centered at $g = 2.20$ corresponds to fine structure transitions of the $S^T = 2$ state, and the doublet at the larger g value (lower field) corresponds to the perpendicular transitions of the $S^T = 1$ state. While the results are somewhat approximate, due to a lack of knowledge of other possible excited states, computer simulation of the Q-band spectrum (dashed line in Figure 16) agrees to within experimental error. The magnetic parameters are summarized in Table 3.

We note that the $g_\perp$ value (2.550) for the $S^T = 1$ state of $\mathbf{K_7Na}$**-1** is unusually large for a Cu^{2+} system. This might be a result of the fact that there are several states in close proximity to the $S^T = 2$ levels, and hence, the standard notion of the effective spin Hamiltonian might not be valid. This point thus needs further investigation.

Conclusions

We have synthesized and structurally characterized the novel tetra-copper-substituted heteropolyanion **1**. The title

(27) Solanki, N. K.; McInnes, E. J. L.; Mabbs, F. E.; Radojevic, S.; McPartlin, M.; Feeder, N.; Davies, J. E.; Halcrow, M. A. *Angew. Chem., Int. Ed.* **1998**, *37*, 2221.

polyanion **1** represents the first tetrasubstituted member of the class of lone-pair-containing, transition-metal-substituted, sandwich-type polyoxoanions. It is closely related to the tri-copper-substituted derivatives **2** and **1a**. The former exhibits ideal D_{3h} symmetry, whereas the latter is a distorted species with C_s symmetry. It seems that the ratio of Cu^{2+}/AsW_9O_{33} plays an important role, but so do the different counterions (Na^+ vs K^+). The latter underlines once again the important role of cations in polyanion synthesis and crystallization. With the current work we showed that the tri-copper-substituted species **1a** can be stabilized by incorporation of an additional copper(II) ion instead of a potassium ion, resulting in **1**. Our results also indicate that the dimeric, sandwich structural type of **1**, **1a**, and **2** is stabilized better by copper(II) ions than any other first-row transition metal. Currently, we are investigating if the antimony(III), selenium(IV), and tellurium(IV) derivatives of **1** can also be synthesized. Meanwhile, we have isolated a derivative of **1** containing five copper(II) centers, which will be reported shortly. Currently, we are in the process of investigating if even six copper(II) ions can be incorporated into the above structural type, which would represent the first Cu_6-crown-substituted polyoxometalate.

The unique arrangement of the four copper(II) centers in **1** results in a novel magnetic exchange fragment in polyoxoanion chemistry. Our magnetic studies support the X-ray structure and also provide insight into the magnetic exchange within the Cu_3 trimer in **2** and the Cu_4 tetramer in **1**. Magnetic susceptibility and EPR studies show that **Na**$_9$**-2** has antiferromagnetically coupled Cu^{2+} ions, while **K**$_7$**Na-1** has both ferromagnetically and antiferromagnetically coupled Cu^{2+} ions. However, in both compounds the dominant antiferromagnetic interactions result in ground-state spins of $S^T = 1/2$ in **Na**$_9$**-2** and $S^T = 1$ in **K**$_7$**Na-1**. In summary, our studies show that the magnetic and electronic properties of **K**$_7$**Na-1** and **Na**$_9$**-2** are markedly different from each other, in contrast to what has been reported in the literature.[14,15] Moreover, these polyanions are some of the rarest ones wherein one is able to fully characterize by EPR the ground state as well as the excited spin levels. We believe that this study will elicit further theoretical as well as synthetic investigations.

Acknowledgment. X-ray measurements were made during a visit of U.K. to the laboratory of Prof. M. T. Pope at Georgetown University. U.K. thanks the Georgetown University Chemistry Department for allowing use of the X-ray diffractometer. Figures 1−7 were generated by Diamond Version 2.1b (copyright Crystal Impact GbR).

Note Added after ASAP: This paper was posted ASAP on December 9, 2003, with incorrect author affiliation indicators. The version posted on December 17, 2003, contains the correct indicators.

Supporting Information Available: One X-ray crystallographic file in CIF format. This material is available free of charge via the Internet at http://pubs.acs.org.

IC034697B